Chinese Chemical Letters 36 (2025) 110281

Contents lists available at ScienceDirect

Chinese Chemical Letters

journal homepage: www.elsevier.com/locate/cclet

Ionic exchange based intracellular self-assembly of pitaya-structured nanoparticles for tumor imaging

Hao Zhang[1], Hao Liu[1,*], Ke Huang, Qingxiu Xia, Hongjie Xiong, Xiaohui Liu, Hui Jiang*, Xuemei Wang*

State Key Laboratory of Digital Medical Engineering, School of Biological Science and Medical Engineering, Southeast University, Nanjing 210096, China

ARTICLE INFO

Article history:
Received 23 April 2024
Revised 13 July 2024
Accepted 17 July 2024
Available online 18 July 2024

Keywords:
Fluorescence
Self-assembly
Biomineralization
Au nanoclusters
Protein coronas

ABSTRACT

The potential of metal nanoclusters in biomedical applications is limited due to aggregation-caused quenching (ACQ). In this study, an *in situ* self-assembled pitaya structure was proposed to obtain stable fluorescence emission through protein coronas-controlled distance between gold nanoclusters (Au NCs). Interestingly, the gold ion complexes coated with proteins of low isoelectric point (pI) nucleate at the secondary structure of proteins with high pI through ionic exchange within cells, generating fluorescent Au NCs. It is worth noting that due to the steric hindrance formed by the protein coronas on the surface of Au NCs, the distance between Au NCs can be controlled, avoiding electron transfer caused by close proximity of Au NCs and inhibiting fluorescence ACQ. This strategy can achieve fluorescence imaging of clinical tissue samples without observable side effects. Therefore, this study proposes a distance-controllable self-assembled pitaya structure to provide a new approach for Au NCs with stable fluorescence.

The application of fluorescent materials in biological fluorescence imaging is limited by the phenomenon of fluorescence quenching, especially aggregation-caused quenching (ACQ) at high concentrations [1–3]. The gradual weakening or even disappearance of the fluorescence signal will lead to the decrease of the signal-to-noise ratio, and reduce the detection sensitivity and dynamic range [4]. ACQ also makes the fluorescence signal spatially blurred, which reduces the imaging resolution and affects the ability to observe and analyze fine structures or local areas [5]. Quantitative analysis or location identification of target substances by fluorescence imaging will be interfered by ACQ, which may lead to misjudgment and data bias, increasing the uncertainty of experimental results [6–8]. Therefore, ACQ is still one of the difficult problems to be solved in fluorescence bioimaging [9,10].

Due to ultra-small size and good biocompatibility, gold nanoclusters (Au NCs) have attracted much attention as excellent fluorescent probes [11,12]. Although Au NCs have higher brightness and longer life than traditional fluorescent dyes, passive aggregation between Au NCs can lead to fluorescence quenching, which affects the imaging effect [13]. Hence, the search for fluorescent substances that can release stable fluorescence is still an important prerequisite for developing fluorescence imaging applications [14,15].

It is one possible breakthrough that Au NCs can be combined with different surface modifiers to achieve improved performance, including fluorescence intensity and stability [16]. Since the luminescence effect of Au NCs is affected by the distance between Au NCs, it is a feasible method to prevent Au NCs from ACQ by synthesizing specific structures to increase the distance between Au NCs [17]. Lu *et al.* used the sulfhydryl modified covalent organic frameworks (COFs) as the carrier of the Au NCs to achieve the anchor deposit Au NCs and inhibit their growth, so that it still has a stable luminescence under long-term *in situ* light [18]. Although the biological applications of this study are limited by the poor biocompatibility and biodegradability of COFs, it still can be considered as a feasible method to prevent direct contact between Au NCs by a stable protective layer comprised of appropriate surface modifiers [19].

Among many synthesis methods, self-assembly is considered a potential method to synthesize protected Au NCs due to its high efficiency, stability, and tunability [20–22]. The effective protection and manipulation of Au NCs can be achieved by selecting the surface modifier and controlling the self-assembly process, which makes it feasible to form a stable protective layer on the surface of Au NCs [23]. Guo *et al.* combined polypeptides with gold ions to

* Corresponding authors.
E-mail addresses: lhaoiu8327@126.com (H. Liu), sungi@seu.edu.cn (H. Jiang), xuewang@seu.edu.cn (X. Wang).
[1] These authors contributed equally to this work.

https://doi.org/10.1016/j.cclet.2024.110281
1001-8417/

enhance the enrichment ability of Au NCs in bacteria through electrostatic interaction, but such enrichment made the fluorescence of Au NCs unstable [24]. Liu *et al.* synthesized Au NCs using DNA as a template. This method can effectively control the emission light of Au NCs. Although the luminescence of Au NCs has been improved, the possible ACQ has not been avoided [25].

Notably, some researchers have found that special structures similar to pitaya is robust, but the application of such structures to biofluorescence imaging is still rare [26,27]. In this structure, the nanoparticles can be protected by certain media, thus maintaining a suitable distance from each other, which prevents ACQ of nanoparticles [28]. In our past work, we hypothesized that intracellular biomineralized anisotropic gold nanocrystals nucleate, crystallizes, and grows in the secondary structures of proteins [29,30]. In addition, different protein molecules have different ion selectivity, and ions are more inclined to bind to protein molecules with strong affinity, resulting in ionic exchanges [31–33]. Gold ions can undergo ionic exchange between proteins at different isoelectric points (PI), and then some proteins will be attached to the surface of the reduced Au NCs. So, it is a feasible strategy to form protein-coated Au NCs with a pitaya-like structure by *in situ* self-assembly [34]. In the meantime, the biocompatibility of Au NCs is enhanced by the protein coronas on their surfaces [35].

Here, a simple and effective strategy for the formation of pitaya-structured gold nanoclusters (PSACs) is designed by *in situ* self-assembly (Fig. S1 in Supporting information). The Au NCs coated with media proteins can isolate NCs from each other and prevent the ACQ effect, to ensure the intracellular stability during applications. To evaluate the fluorescence stability of PSACs, the emission of PSACs under different conditions was also examined. Furthermore, the mechanism of PSACs formation is also studied in this article, which may be based on ionic exchange between proteins. Therefore, this study is conducive to the further application of fluorescent nanomaterials in biological detection.

In the process of experiment, the egg whites (EW) were separated from sterile eggs and chlorauric acid ($HAuCl_4$) was added to the aqueous solution of the EW (EW@Au(I)). The physicochemical properties of EW@Au(I) and EW are basically the same, presenting as a colorless and transparent liquid, soluble in water, and a protein molecule that forms alloy ions. The EW@Au(I) solution was incubated with A549 cells for 24 h and eventually Au NCs were formed in the cells by *in-situ* self-assembly. The Au NCs were isolated from the cells by repeated freeze-thaw and differential centrifugation.

The morphology and size of Au NCs extracted from the cells were characterized by transmission electron microscopy (TEM). The TEM image shows that the Au NCs are encased within medium forming a pitaya-like structure (PSACs) (Fig. S2 in Supporting information). The statistical results show that the PSACs have a size between 100 nm and 220 nm. More detailed TEM image of the PSACs shows the assembly of ultrasmall particles in the structure (Fig. 1a). The results of selected area electron diffraction (SAED) show that the gold nanostructure belongs to the amorphous state (Fig. S3 in Supporting information). The dark-field TEM image of PSACs provides further evidence that the Au NCs are coated in proteins, with an appropriate distance among NCs (Fig. 1b). The particle size statistics of NCs in PSACs were performed as shown in Fig. 1c. The results confirm a relatively narrow size distribution around 2.6 nm, which allows the PSACs to have stable fluorescent properties. The distance between Au NCs ranges from 2.5 nm to 10.5 nm, with a medium distance at about 6 nm (Fig. S4 in Supporting information). Therefore, this structure may be beneficial in preventing fluorescence quenching of Au NCs due to aggregation. Confocal laser scanning microscopy (CLSM) dark-field imaging of the extracted PSACs was also performed (Fig. 1d). The size of PSACs is about between 100 nm and 200 nm, which is consistent with the

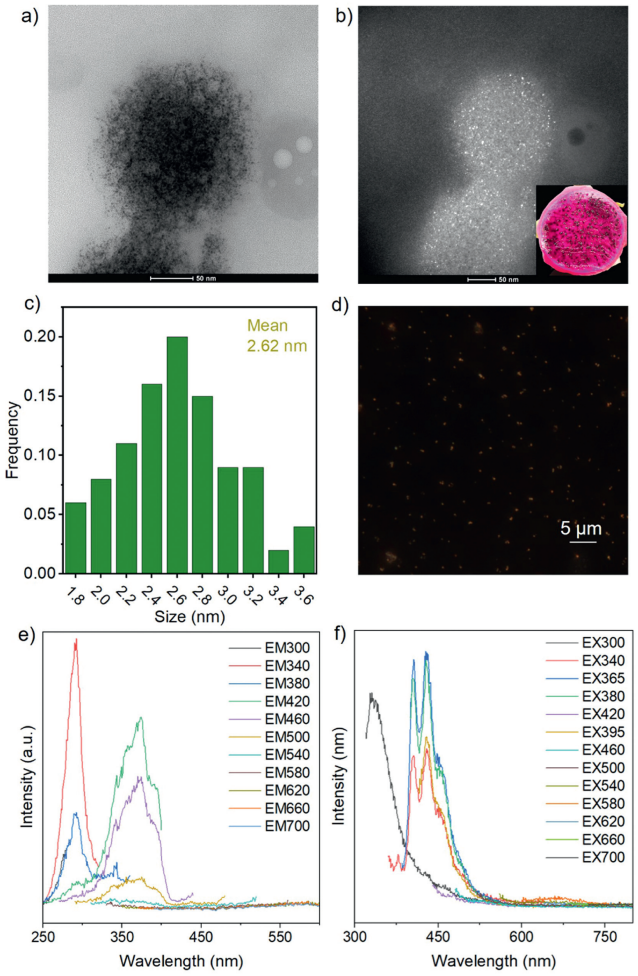

Fig. 1. The characterization of intracellular PSACs. (a) TEM images of PSACs. (b) Dark-field TEM image of PSACs. Scale bar: 50 nm. (c) The size histogram of Au NCs in PSACs. (d) CLSM dark-field image of PSACs. Scale bar: 5 μm. The excitation (e) and emission (f) spectra of PASCs under various wavelengths.

statistical results of TEM images. Besides, the results showed that PSACs had good reproducibility through five independent repeated experiments (Fig. S5 in Supporting information).

The Fourier transform infrared spectroscopy (FT-IR) of EW and PSACs are depicted in Fig. S6 (Supporting information). For both samples, the peaks at 1085 cm^{-1} (-C-O-), 1160 cm^{-1} (-COO-), 1537 cm^{-1} (-C=C-), 1656 cm^{-1} (-COOH), and 2957 cm^{-1} ($-CH_3$) are present. Ester groups are widely found in peptide bonds in proteins, while other chemical bonds exist in the side chains of proteins. Raman spectroscopy is used to verify the chemical bonds on PSACs (Fig. S7 in Supporting information). The results are consistent with the FT-IR results, and there is a vibrational peak attributed to peptide bonds in PSACs at 1300 cm^{-1}. This proves that Au NCs are encapsulated by proteins, which may give the PSACs greater stability than dispersed Au NCs. Due to the barrier of protein coronas between Au NCs, the steric hindrance between Au NCs increases, and it is difficult for Au NCs to approach each other. So, the size of Au NCs does not increase to the point that the quantum size effect is lost, which ensures that the fluorescence emission of PSACs is very stable.

The molecular structure and valence of PSACs are illustrated by X-ray photoelectron spectroscopy (XPS). The structure contains the elements C, N, O, P, and Au (Fig. S8a in Supporting information). The molecular orbitals associated with the Au element encompass Au $4f_{5/2}$ and Au $4f_{7/2}$, and the valence states of the elements are

Au(0) and Au(I), which suggests that PSACs contain reduced Au NCs (Fig. S8b in Supporting information). The elements C, N, and O, especially C, may be mainly derived from the protein coronas in PSACs (Fig. S8c in Supporting information).

The optical characterization of PSACs was performed by ultraviolet–visible spectroscopy (UV–vis) and fluorescence spectroscopy. The UV–vis absorption spectra show an absorption peak at 280 nm, which is due to the presence of protein in EW@Au(I) and PSACs (Fig. S9 in Supporting information). And it was found that PSACs has a weak absorption at 365 nm, possibly due to the metal-ligand charge transfer effect. In the fluorescence spectroscopy (Figs. 1e and f), the optimal fluorescence excitation wavelength for PSACs is 365 nm, and the optimal emission wavelength is 420 nm. This indicates that PSACs absorbs energy at a wavelength of 365 nm and emits fluorescence through radiative transitions. The zeta potential of PSACs is approximately 37 mV. This means that there is a large repulsive force between PSACs, which makes PSACs have good stability (Fig. S10 in Supporting information). In order to check the optical stability of PSACs, the emission spectrum under different conditions was successively measured upon excitation at 365 nm. At 25 °C, the fluorescence intensity of PSACs remained unchanged after repeated excitation for 10 times, which indicates a high resistance to photobleaching (Fig. S11 in Supporting information). When the temperature is adjusted to 4 °C or 60 °C, the emission peak of PSACs remains at 420 nm after repeated excitation (Fig. S12 in Supporting information). By comparing the fluorescence intensity under different temperatures, the fluorescence intensity change caused by temperature is very weak (Fig. S13 in Supporting information). The response of PSACs to temperature may be related to the protein coronas covering the Au NCs.

The fluorescence stability of PSACs under different ionic strength was further studied by titration with saturated solution of NaCl (Fig. S14 in Supporting information). Upon excitation at 365 nm, the emission wavelength of PSACs is still around 420 nm in the presence of different concentrations of saline. The fluorescence intensity show slight increase before reaching a plateau. In general, PSACs still have stable fluorescence emission at 420 nm under different ionic strength.

Proteins can be denatured at rigorous pH, which may have an effect on the fluorescence properties of the PSACs. Actually, PSACs still has stable emission at 420 nm under acidic or neutral conditions (Fig. S15 in Supporting information). The fluorescence intensity of PSACs do not show significant difference between pH 3 and 7.4. However, at pH 9, the fluorescence intensity of PSACs was significantly improved, which was four times higher than that at pH 7.4 (Fig. S16 in Supporting information). This may be due to changes in the charge state and solubility of the protein coronas under alkaline conditions which increases the distance between Au NCs. As shown in Fig. S17a (Supporting information), the longer distance reduces the interaction between the Au NCs, alleviates the localized fluorescence quenching effect, and enhances fluorescence stability. When the distance between the Au NCs is too close, the energy of the Au NCs transition from the excited state to the ground state cannot be released in the form of photons, so it can only be released in the form of heat, and a non-radiative transition occurs (Fig. S17b in Supporting information).

In order to better explain the excitation and emission of the PSACs at 280 and 360 nm, the excitation and emission spectra of EW were respectively detected (Fig. S18 in Supporting information). This result successfully proved that the excitation peak of the PSACs at 280 nm and the emission peak at 340 nm were attributed to proteins. Further exploration showed there was no difference in fluorescence properties between EW and EW@Au(I) (Fig. S19 in Supporting information). This indicates that gold ions will not be reduced to Au NCs by EW under neutral conditions. Then the effect on EW@Au(I) by polar molecules was studied. The excitation spectrum and emission spectrum are similar before and after adding PEG8000 to EW@Au(I) (Figs. S20a and b in Supporting information). So the effect of polar molecules can be excluded.

Some groups have indicated that by adjusting pH, EW can reduce gold ions [36–38]. Therefore, the formation of Au NCs in EW@Au(I) solution at different pH were investigated (Figs. S20c and d in Supporting information). Under acidic and neutral conditions, only the absorption peak near 280 nm for proteins is present in the UV–vis spectra. On the contrary, under alkaline conditions, the absorption peaks around 365 and 600 nm appear, indicating the reduction of Au(III) ions. It means that the reduction of EW-protected gold ions can be affected by pH.

Considering that the charges of proteins are closely related to pH, and the isoelectric point (pI) of ovalbumin, which accounts for a large proportion in EW, is low (∼4.6), the effect of protein with higher pI on EW@Au(I) was explored. Lysozyme (Lysm), with an pI of 10.5 was chosen due to the considerable abundance in EW. Notably, the addition of Lysm to EW@Au(I) (EW@Au(I)@Lysm) has been shown to promote the reduction of gold ions to Au NCs. As shown in the excitation and emission spectra of EW@Au(I)@Lysm (Figs. S20e and f in Supporting information), it emits blue fluorescence at about 420 nm upon excitation at 360 nm, which is very similar to the fluorescence properties of PSACs. Therefore, we speculate that proteins with high pI in cells play an important role in the *in-situ* synthesis of PSACs in A549 cells.

To further prove our hypothesis and to verify whether ovalbumin in egg white plays a major role, EW was replaced with pure ovalbumin (Ova@Au(I)@Lysm) for testing. The experimental results for Ova@Au(I)@Lysm are consistent with those of EW@Au(I)@Lysm (Figs. S20g and h in Supporting information), suggesting that ovalbumin and lysozyme play important roles in the whole reaction process of EW@Au(I)@Lysm. This also means that the synthesis of PSACs may be caused by the separation of gold ions from ovalbumin due to ionic exchange. Then it exchanges to proteins with higher pI in the cell to nucleate and grow into Au NCs, which can be further wrapped by protein coronas to form PSACs with stable fluorescence. In Fig. S20i (Supporting information), the UV–vis spectrum of Ova@Au(I)@Lysm at 280 and 360 nm is also very similar to the absorption peak of PSACs, which further supports our conjecture. The molecular docking simulation of gold ions with ovalbumin and lysozyme was used to further test our theory (Figs. S20j and k in Supporting information). Although gold ions tend to attach to the corner of the β-turn in the secondary structure of Ova and Lysm, the binding energy of Lysm and gold ions is higher than that of Ova and gold ions, which makes gold ions more inclined to bind to Lysm with high pI.

Although the fluorescence stability of PSACs under different conditions has been demonstrated, the biosafety of PSACs still requires consideration when applying for fluorescence imaging of tumor cells. Under the fixed EW content, EW@Au(I) with different concentrations of $HAuCl_4$ (0, 16, 32, 48, 64, and 80 μmol/L) was incubated with A549 cells and BEAS-2B cells for 24 h respectivily. The cell viability was ∼100% with the increase of $HAuCl_4$ concentration in EW@Au(I) (Fig. 2a and Fig. S21 in Supporting information). For the cell viability staining experiments (Fig. 2b), only a small ratio (∼1%) of A549 cells were stained, indicating that EW@Au(I) has a negligible cytotoxicity. The $HAuCl_4$ concentration of 32 μmol/L was selected for the preparation of PSACs.

Since PSACs has good biocompatibility and excellent fluorescence stability, the application of PSACs in cell and tissue imaging were further studied. The CLSM dark-field imaging was used to measure PSACs in A549 cells. As shown in Fig. 2c, PSACs was produced in A549 cells co-incubated with EW@Au(I), but not in the control group without EW@Au(I). The generated PSACs is mainly present in the cytoplasm, but not in the nucleus, indicating that

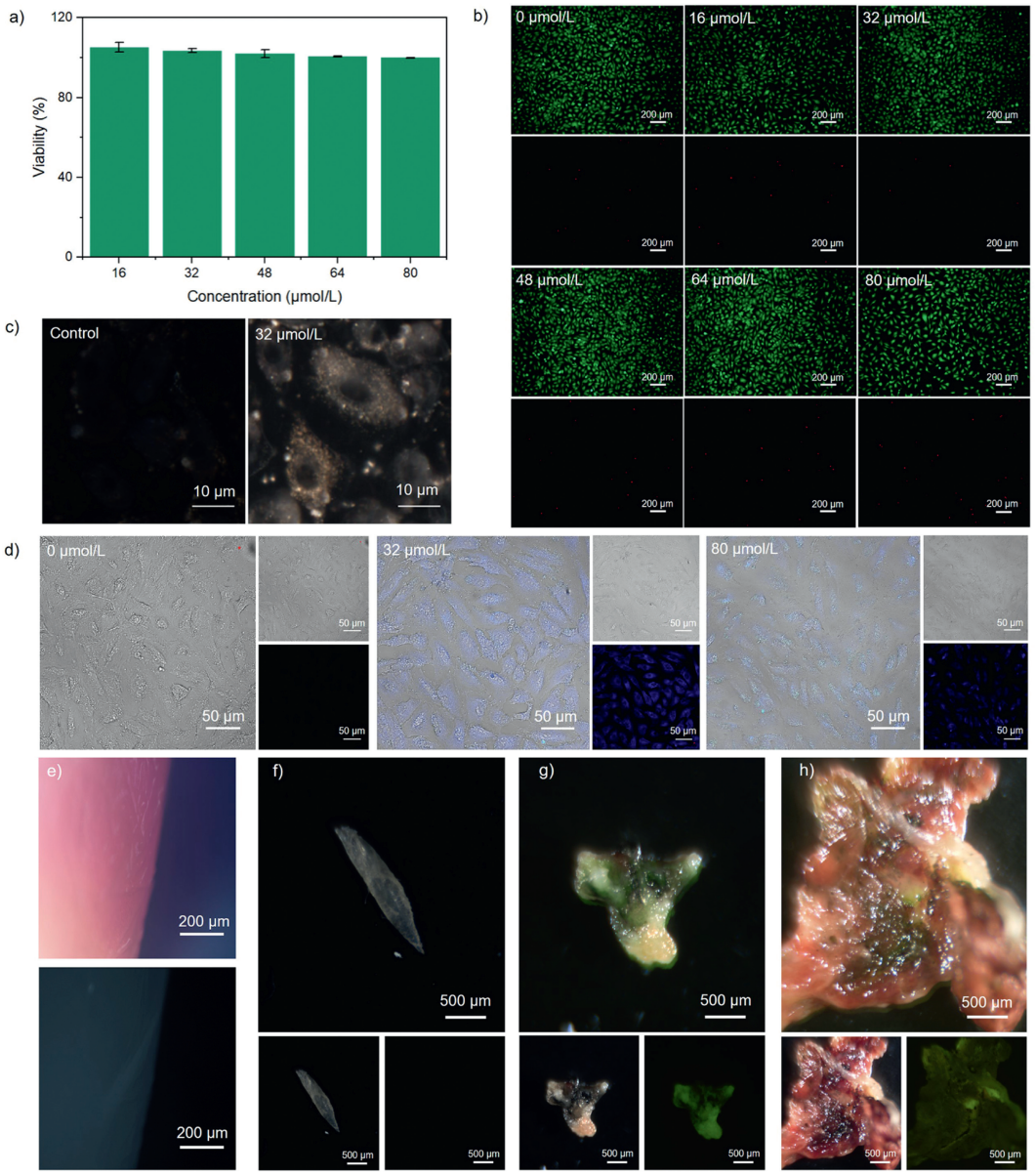

Fig. 2. The imaging of cells and tissues. (a) CCK-8 assay and (b) viability staining of A549 cells 24 h after the cells were cultured with various concentrations of EW@Au(I) (0, 16, 32, 48, 64 and 80 μmol/L). Scale bar: 200 μm. (c) CLSM dark-field image of A549 cells. Scale bar: 10 μm. (d) The fluorescence imaging of A549 cells after the cells were cultured with various concentrations of EW@Au(I) (0, 32, and 80 μmol/L) for 24 h. Scale bar: 50 μm. (e) The imaging of mice tumors. Scale bar: 200 μm. (f) The imaging of human epithelial tissue. Scale bar: 500 μm. (g, h) The imaging of pulmonary tuberculosis tissue. Scale bar: 500 μm.

proteins in the cytoplasm play an important role in the formation of PSACs. Next, the effect of $HAuCl_4$ concentration in EW@Au(I) on the formation of PSACs in A549 cells was studied by CLSM (Fig. 2d). PSACs was formed in A549 cells after adding EW@Au(I), and blue fluorescence was produced under ultraviolet excitation. At the same time, the group with $HAuCl_4$ concentration of 32 μmol/L exhibited enhanced blue fluorescence than that with $HAuCl_4$ concentration of 80 μmol/L. The reason may be that the proteins involved in the formation of protein coronas in cells are limited, and the increased concentration of $HAuCl_4$ causes the wrapping of more Au NCs in limited protein coronas. This means that the Au NCs in the PSACs are forced closer together, resulting in a weakening of the blue fluorescence. In addition, we performed long-term cell tracking experiments. The fluorescence of PSACs was observed in A549 cells at different incubation times by CLSM (Fig. S22 in Supporting information). When the incubation time reached one hour, the cells showed weak fluorescence. When the co-incubation time reached 24 h, the fluorescence had best intensity (Fig. 2d (middle) and Fig. S22 in Supporting information).

Subsequently, the possibility of applying PSACs to fluorescence imaging in tumor lesion tissues was also explored. Mice were used in the experiment from southeast university laboratory animal center with approval. Animal experiments were approved by the Ethics Committee of Southeast University. After mouse tumor tissue was immersed in EW@Au(I) for 24 h, stereoscopic fluorescence microscope images showed that tumor tissues showed conspicuous blue fluorescence (Fig. 2e). However, it did not change significantly in normal tissue, meaning that EW@Au(I) was more likely to be reduced to form PSACs in tumor cells (Fig. S23 in Supporting information). Then, the potential of this method for the detection of human tumor biopsy samples was validated. The stereoscopic fluorescence microscope images of human tissues show that it emits strong green fluorescence in human tumor tissues (Figs. 2g and h), but not in normal tissues (Fig. 2f). This indicates that it

is feasible to apply PSACs to the sample detection of human tumor biopsy. The reason why the fluorescence of biopsy samples of human tumors is green may be that some substances in the tissue can absorb the blue fluorescence by PSACs, which leads to the energy transfer, which in turn produces the green fluorescence emission. Nevertheless, the difference in fluorescence imaging results between normal tissues and tumor tissues still supports the possibility of applying PSACs to the preliminary detection of tumor biopsy tissue samples.

In summary, we have demonstrated a strategy about intracellular self-assembly of PSACs. In PSACs, Au NCs in the size of 2–3 nm are coated by protein coronas, which prevent them from aggregating with each other, thus avoiding aggregation-induced fluorescence quenching. The PSACs has also been shown to have excellent fluorescence stability under different conditions. It should be noted that the formation mechanism of PSACs in our study was revealed, which was based on gold ionic exchange between proteins with lower and higher pI. The Au NCs nucleates on the secondary structure of the proteins. Furthermore, when PSACs were used for fluorescence imaging of A549 cells, it showed good luminescence stability and biocompatibility. The effect of co-incubation time and ionic concentrations on cell fluorescence imaging was demonstrated. The probe shows specificity to tumor tissue and can distinguish tumor tissue from normal tissue by fluorescence imaging results. This study reveals the mechanism of intracellular self-assembly of PSACs and suggests that the PSACs may be used as a probe candidate for fluorescence imaging of tumor cells and tissues, which will facilitate the early diagnosis of cancer.

Ethical statement

The patients' samples were obtained from Zhongda Hospital of Southeast University. Samples were donated with the patient's consent and approved by the Medical Ethics Committee of Southeast University (No. 82061148012). The study complied with the principles of the Declaration of Helsinki.

Declaration of competing interest

The authors declare that they have no known competing financial interests or personal relationships that could have appeared to influence the work reported in this paper.

CRediT authorship contribution statement

Hao Zhang: Writing – original draft, Investigation. **Hao Liu:** Writing – review & editing. **Ke Huang:** Supervision. **Qingxiu Xia:** Supervision. **Hongjie Xiong:** Project administration. **Xiaohui Liu:** Supervision. **Hui Jiang:** Supervision, Project administration. **Xuemei Wang:** Supervision, Project administration.

Acknowledgments

This work was supported by the National Natural Science Foundation of China (Nos. 82061148012, 82027806, 21974019), SEU Innovation Capability Enhancement Plan for Doctoral Students (No. CXJH_SEU 24138), and Postgraduate Research&Practice Innovation Program of Jiangsu Province (No. KYCX24_0469).

Supplementary materials

Supplementary material associated with this article can be found, in the online version, at doi:10.1016/j.cclet.2024.110281.

References

[1] L. Fang, W.T. Fan, G.Q. Bian, et al., Angew. Chem. Int. Ed. 62 (2023) e202305604.
[2] H. Liu, Y.K. Chen, L.Q. Mo, et al., ACS Nano 17 (2023) 21195–21205.
[3] J.Q. Xin, C.T. Deng, M.C. Zheng, F.F. An, MedComm Biomater. Appl. 2 (2023) e28.
[4] H. Nie, K. Hu, Y.J. Cai, et al., Mater. Chem. Front. 1 (2017) 1125–1129.
[5] X.F. Ma, R. Sun, J.H. Cheng, et al., J. Chem. Educ. 93 (2016) 345–350.
[6] D. Song, C.C. Li, M.T. Zhu, S.Y. Chi, Z.H. Liu, Angew. Chem. Int. Ed. 61 (2022) e202212721.
[7] H. Liu, K. Huang, H. Zhang, et al., Research 7 (2024) 0318.
[8] Y. Yu, M. Pan, J.R. Peng, et al., Chin. Chem. Lett. 33 (2022) 4133–4145.
[9] X.M. Zhou, X.J. Wang, L. Shang, Chin. Chem. Lett. 34 (2023) 108093.
[10] R.F. Han, Y. Xiao, Q.Q. Bai, C.H.J. Choi, Acta Pharm. Sin. B 13 (2023) 1847–1865.
[11] K.Y. Huang, Z.Q. Yang, M.R. Yang, et al., J. Am. Chem. Soc. 146 (2024) 8706–8715.
[12] H. Liu, C. Chen, H.L. Chen, et al., Chem. Eng. J. 446 (2022) 137039.
[13] C. Dai, C.X. Yang, X.P. Yan, Nano Res. 11 (2018) 2488–2497.
[14] H. Liu, Z.M. Liu, J. Xiao, et al., Adv. Healthc. Mater. (2024) 2303248.
[15] H. Liu, H. Jiang, X.H. Liu, X.M. Wang, Exploration 3 (2023) 20230033.
[16] Y.P. Chen, Y.L. Xianyu, X.Y. Jiang, Acc. Chem. Res. 50 (2017) 310–319.
[17] Z.B. Gan, Y.G. Liu, L. Wang, et al., Nat. Commun. 11 (2020) 5572.
[18] Y. Deng, Z. Zhang, P.Y. Du, et al., Angew. Chem. Int. Ed. 59 (2020) 6082–6089.
[19] Q.Y. Tang, G. Zhao, H. Fang, et al., Acta Pharm. Sin. B 14 (2024) 2786–2789.
[20] G.B. Qi, Y.J. Gao, L. Wang, H. Wang, Adv. Mater. 30 (2018) 1703444.
[21] S. Zhang, J.J. Chen, J.L. Liu, et al., Adv. Mater. 33 (2021) 1905784.
[22] S.F. Du, Y. Wang, F.L. Wang, et al., Chin. Chem. Lett. 35 (2024) 109256.
[23] J. Wankar, N.G. Kotla, S. Gera, et al., Adv. Funct. Mater. 30 (2020) 1909049.
[24] Z.C. Guo, J. Xiao, W.W. Liu, et al., Chem. Eng. J. 457 (2023) 141218.
[25] G.Y. Liu, Y. Shao, K. Ma, et al., Gold Bull. 45 (2012) 69–74.
[26] X.J. Xu, J. Liu, Z.B. Liu, et al., ACS Nano 11 (2017) 9033–9040.
[27] N. Zhang, Q. Zhao, X.P. Han, J.G. Yang, J. Chen, Nanoscale 6 (2014) 2827–2832.
[28] A. Yahia-Ammar, D. Sierra, F. Mérola, N. Hildebrandt, X.Le Guével, ACS Nano 10 (2016) 2591–2599.
[29] H. Liu, Z.M. Liu, Y.H. Wang, et al., Adv. Funct. Mater. 33 (2023) 2302136.
[30] M.N. Wang, Z.C. Guo, J.Y. Zeng, et al., Chin. Chem. Lett. 34 (2023) 107651.
[31] J.C. Yang, B.W. Yang, J.L. Shi, Angew. Chem. Int. Ed. (2023) e202310061.
[32] T. Dudev, C. Lim, Chem. Rev. 114 (2014) 538–556.
[33] S.Y. Zhou, Y.J. Li, Q.J. Wu, C.Y. Gong, MedComm Biomater. Appl. 3 (2024) e70.
[34] J. Gao, J. Zhan, Z.M. Yang, Adv. Mater. 32 (2020) 1805798.
[35] C.J. He, T.T. Ye, W.Q. Teng, et al., ACS Nano 13 (2019) 4856–4856.
[36] X.J. Li, J. Ling, C.L. Han, et al., Anal. Sci. 33 (2017) 671–675.
[37] L.L. Li, X. Liu, C.H. Fu, L.F. Tan, H.Y. Liu, Opt. Commun. 355 (2015) 567–574.
[38] D. Joseph, K.E. Geckeler, Colloids Surf. B: Biointerf. 115 (2014) 46–50.